Understanding the Pulsar Multipolar Field Structure through NICER and Fermi data

Constantinos Kalapotharakos
NASA, Goddard Space Flight Center
University of Maryland, College Park

Collaborators
Zorawar Wadiasingh (NASA GSFC)
Alice Harding (Los Alamos National Laboratory, NASA GSFC)
Demos Kazanas (NASA GSFC)

9th International Fermi Symposium

Fermi Gamma-ray Space Telescope

Outline

- **Non-dipolar magnetic fields**
  -*NICER* results (J0030+0451)
- **MCMC, Field Degeneracies**
- **γ-rays**
  -*FERMI* data, FF & dissipative simulations
- **Summary, Future Steps**

Kalapotharakos et al., 2021, ApJ, 907, 63

NICER results

J0030+0451

~20 parameters

Thermal X-ray LC **Bogdanov et al. (2019)**

Riley et al. (2019)

$M = 1.34 M_\odot$
$R = 12.71 km$
$\zeta = 53.85°$

2 hotspots
same temperatures

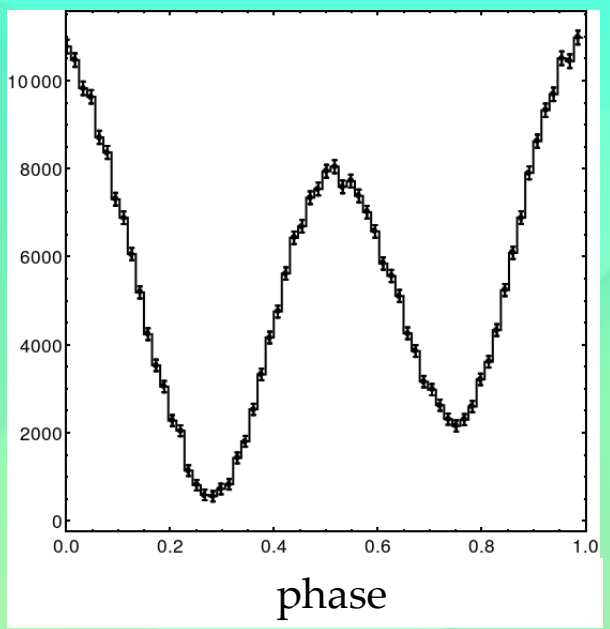

Miller et al. (2019)

$M = 1.49 M_\odot$
$R = 13.64 km$
$\zeta = 47.38°$

2 hotspots
same temperatures
+
3 hotspots

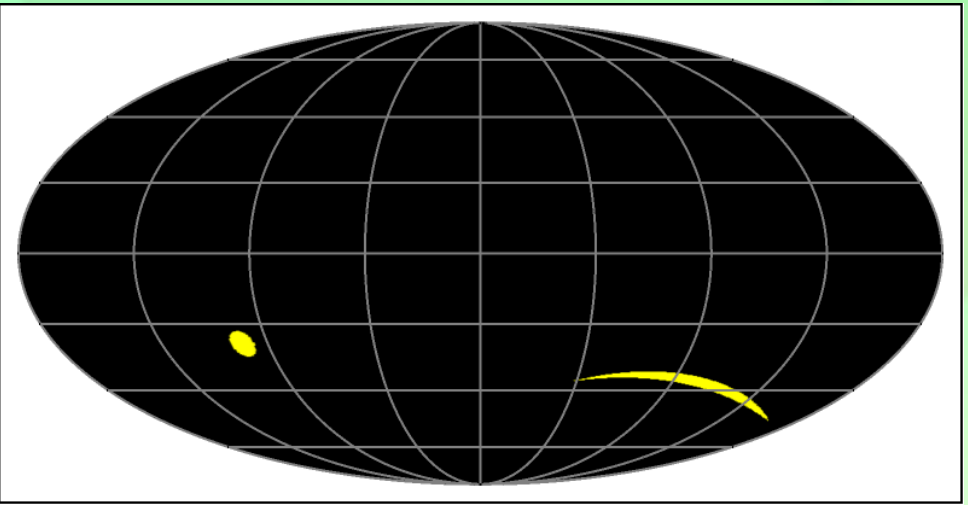

Strong evidence for multipolar magnetic field

Hot spots are based on pre-selected shape patterns unrelated to magnetic field structures

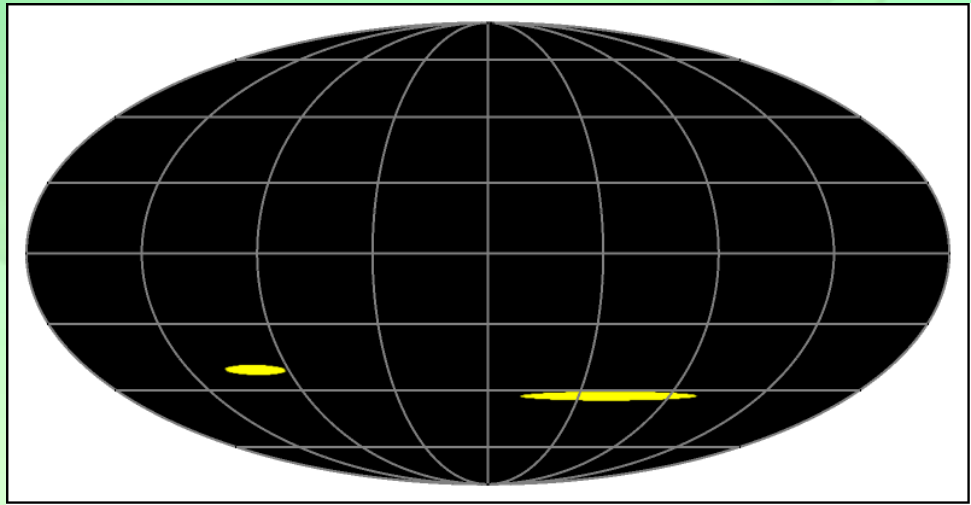

Non-Dipolar Fields

Offset Dipole + Offset Quadrupole

Static Vacuum Field (SVF)

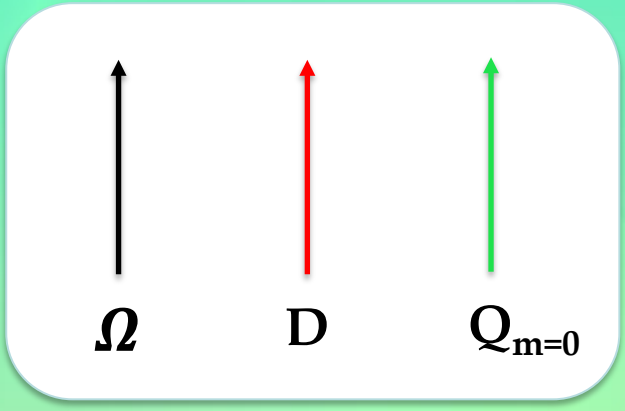

11 parameters

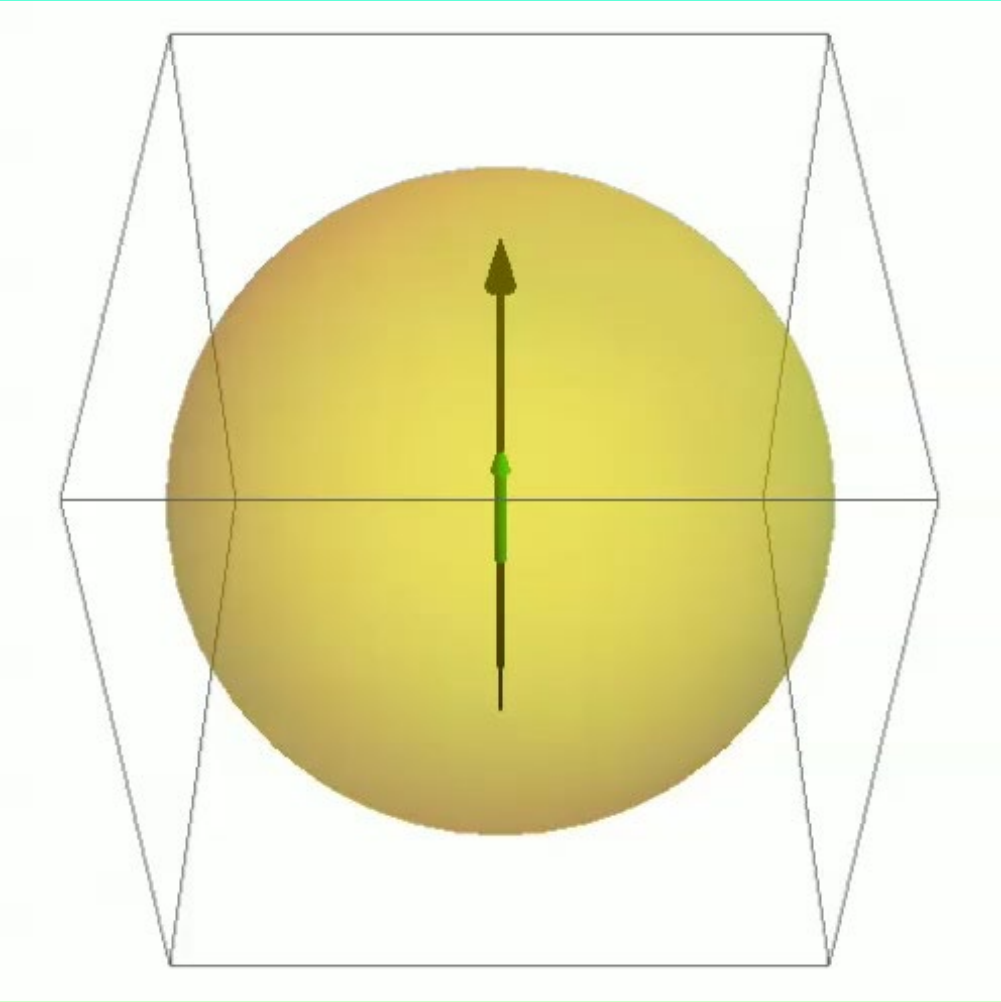

Non-Dipolar Fields
Offset Dipole + Offset Quadrupole

SVF

11 parameters

Central dipole ⟶ offset dipole + offset quadrupole

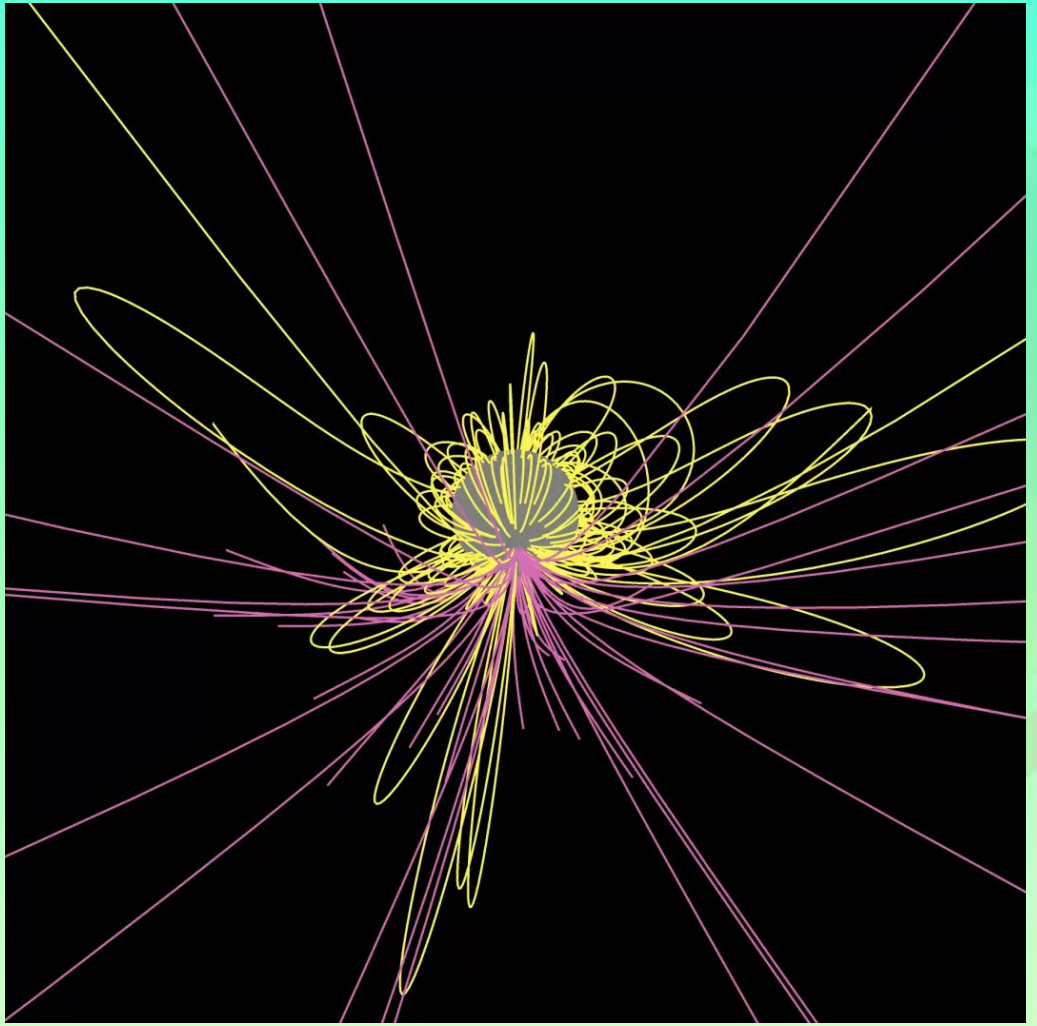

GR Ray Tracing

We developed a **GR-code** (GIKS) that follows the photon trajectories in the full **Kerr-metric**

Kalapotharakos et al. 2021, see Psaltis & Johannsen 2012

We use Kerr metric,
but Schwarzschild metric would be adequate
for PSR J0030 spin rate

$N = 2.5 \times 10^6$

Mathematica, Parallel, Pleiades NASA supercluster

Assumptions
$M_\star, r_\star, \zeta$ from Miller et al. 2019 and Riley et al. 2019

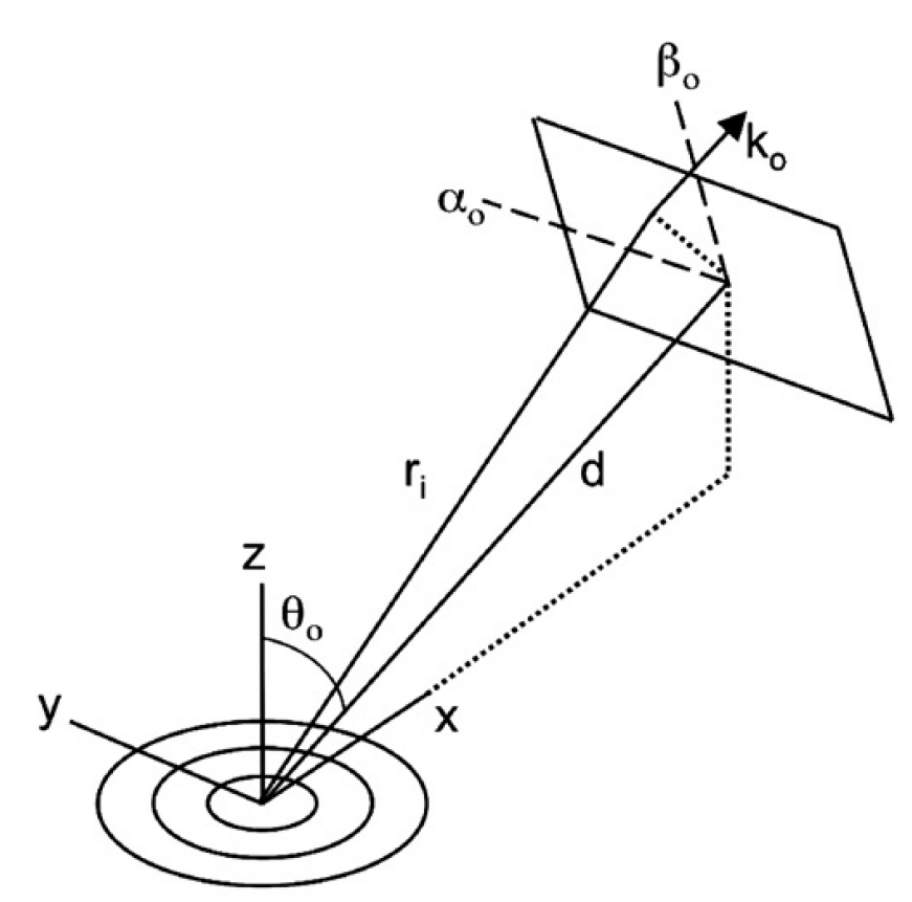

Atmosphere model

The reconstruction of X-ray LCs (i.e., the intensity at each phase) requires the incorporation of the **Doppler boosting** and an **atmosphere model.**

Miller et al. 2019 and Riley et al. 2019 used the same atmosphere model (i.e., pure H^+) even though they used slightly different energy channels.

Atmosphere Model

$$\mathbf{I} = \mathcal{F}(\vartheta_z, E)$$

$$\mathbf{I} \propto \cos^n(\vartheta_z)$$

Assuming the Riley et al. HSs, we were able to reproduce the X-ray LC for $n \approx 1$

Assuming the Miller et al. HSs, we were able to reproduce the X-ray LC for $n \approx 0.65$

Atmosphere model

Atmosphere Model
$\mathbf{I} = \mathcal{F}(\vartheta_z, E)$
$\mathbf{I} \propto \cos^n(\vartheta_z)$

For the Riley et al. HSs, we were able to reproduce the X-ray LC for $n \approx 1$

For the Miller et al. HSs, we were able to reproduce the X-ray LC for $n \approx 0.65$

Projection on the observer plane

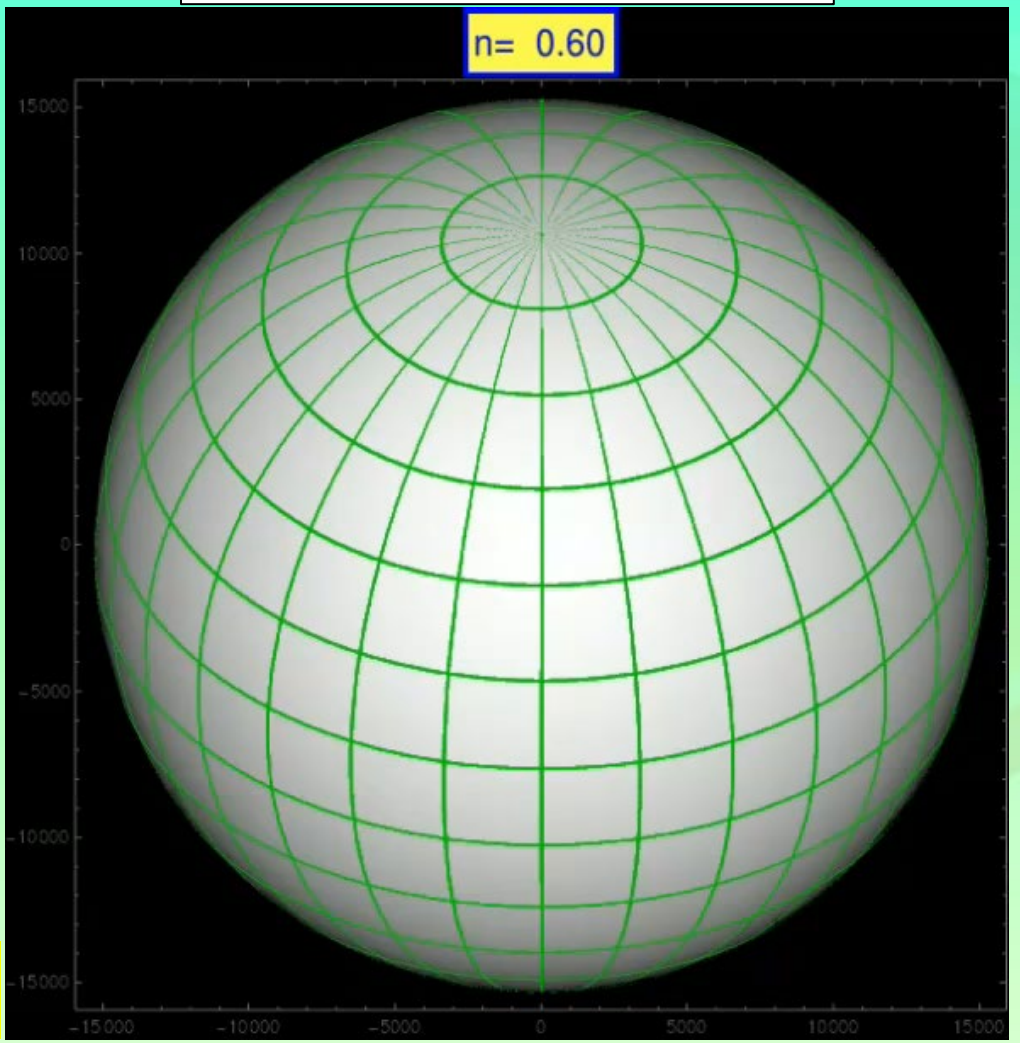

$\zeta = 53.85°$

MCMC exploration

We developed a parallel **MCMC code** implementing the *stretch move* (Goodman & Weare 2010, Foreman-Mackey et al. 2013) ensemble method.

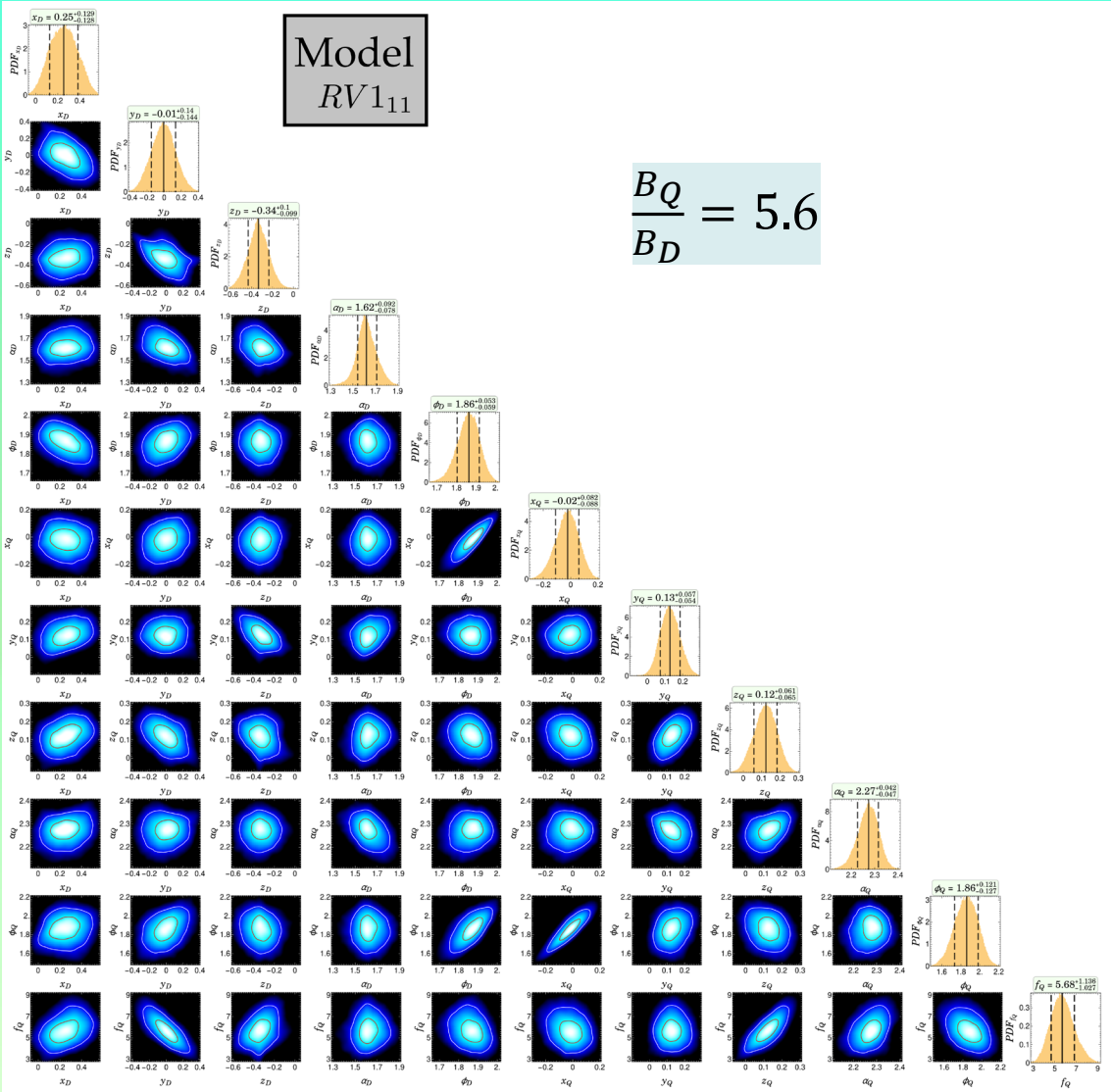

$$\frac{B_Q}{B_D} = 5.6$$

Magnetic Field Solutions

Highest likelihood

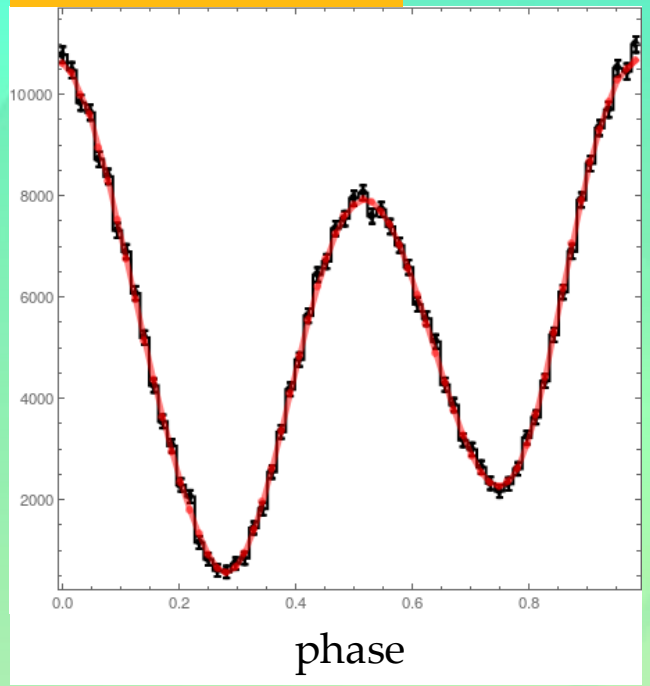

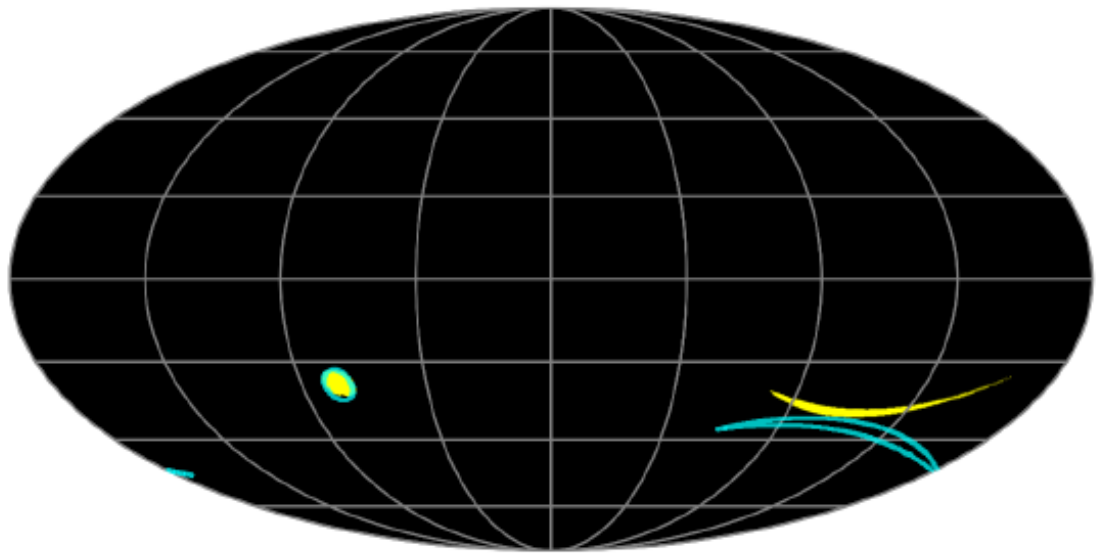

Highest likelihood

$\chi_r^2 = 0.66$

Demonstration

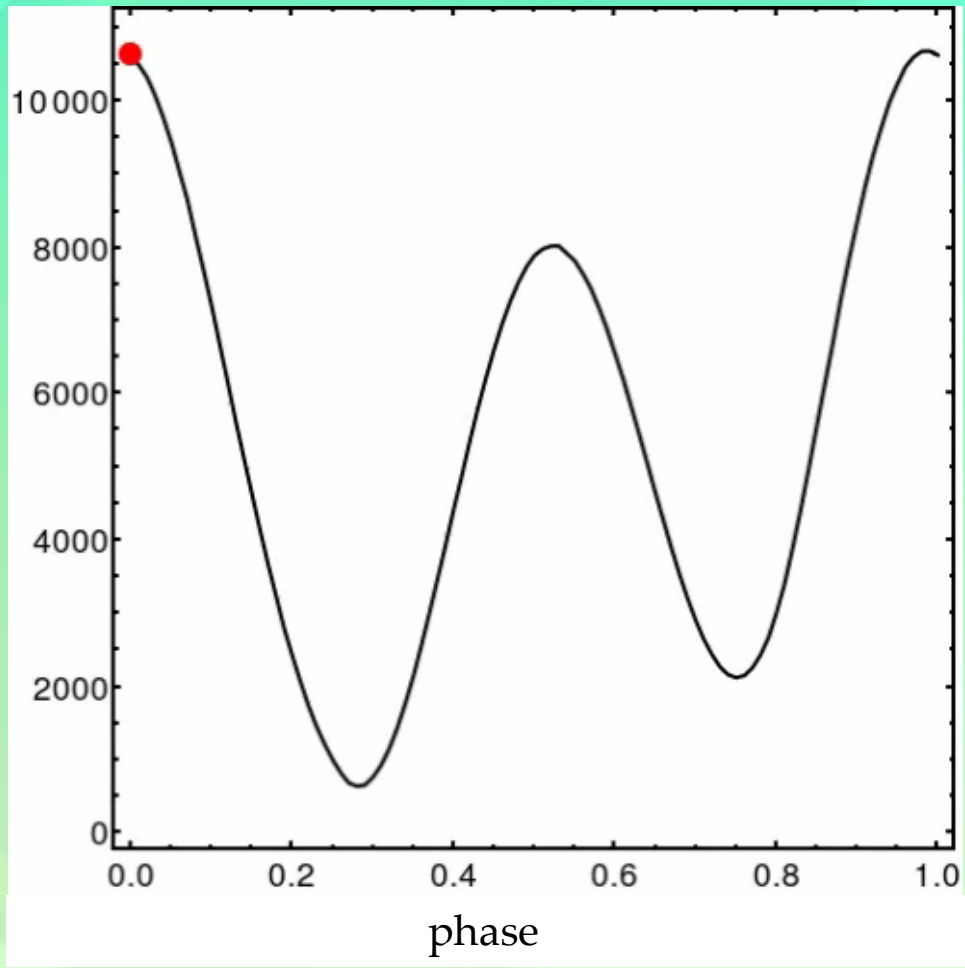

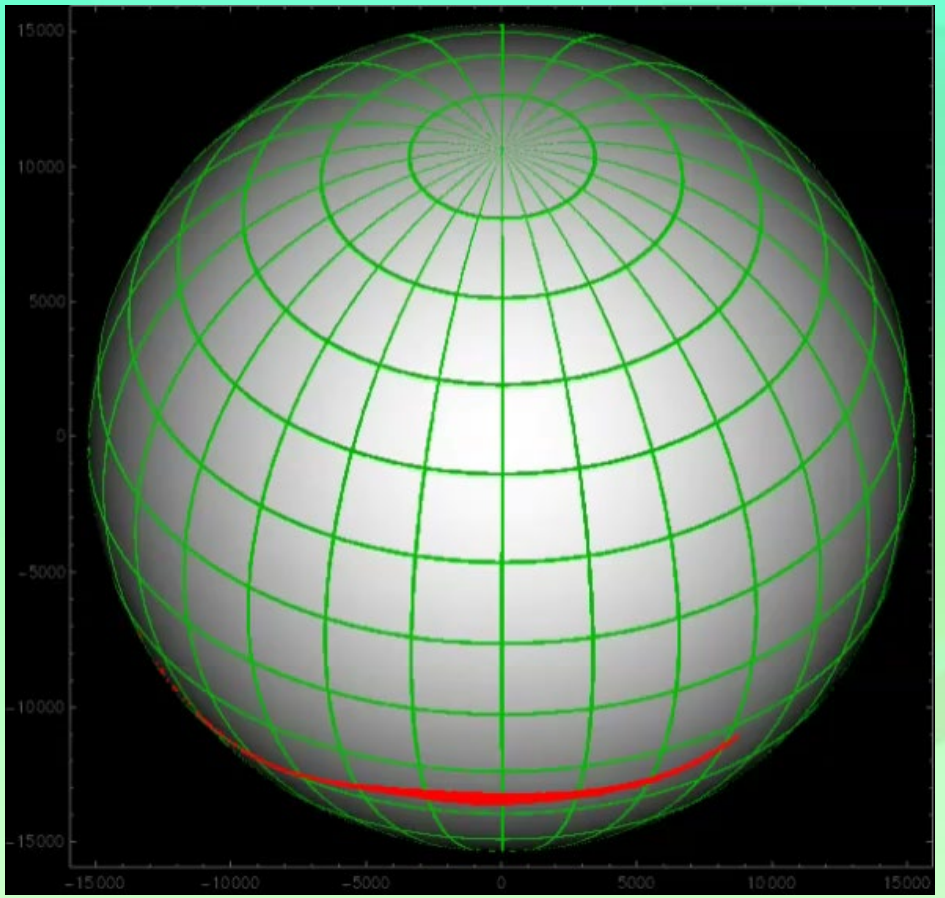

Degeneracies?

Different field configuration

Highest likelihood

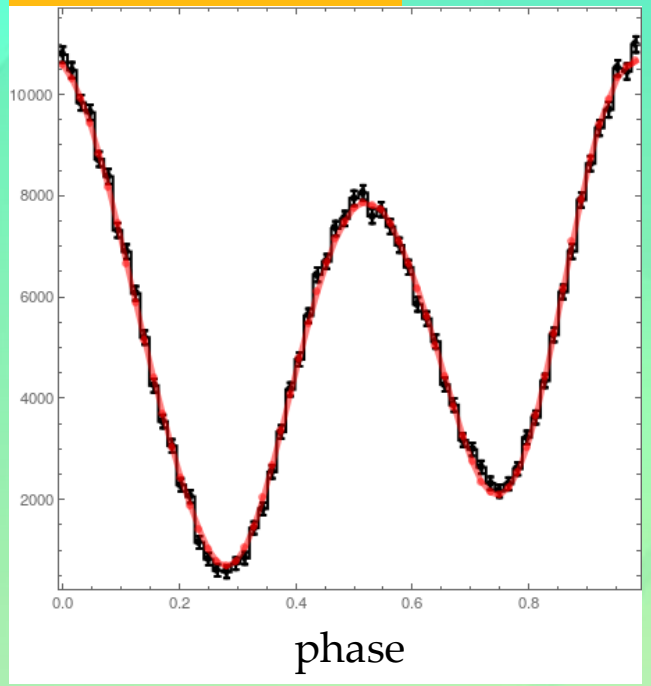

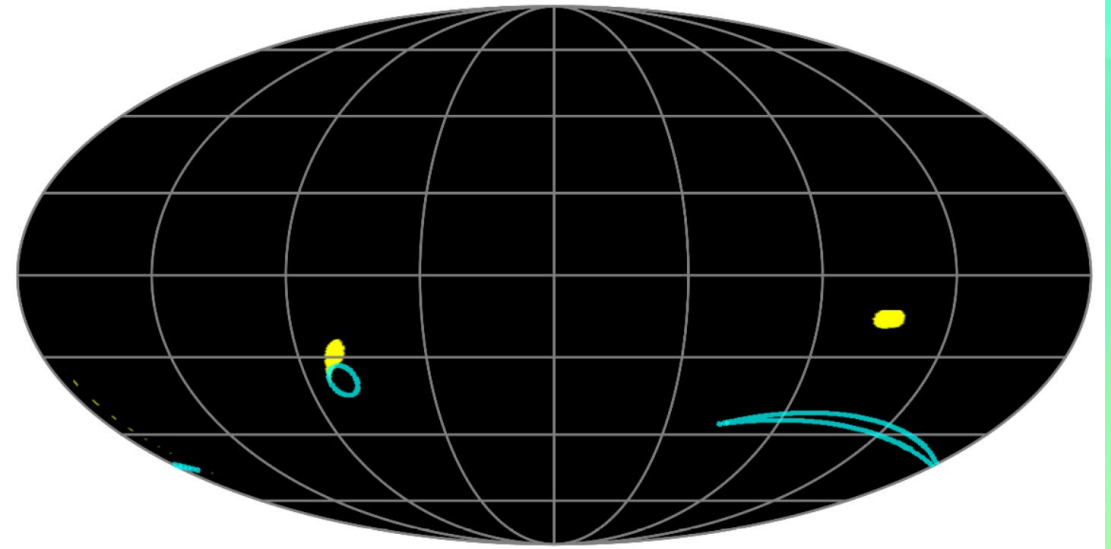

Highest likelihood

$\chi_r^2 = 0.78$

Degeneracies?

SVF, Riley et al., 2019 fixed parameters

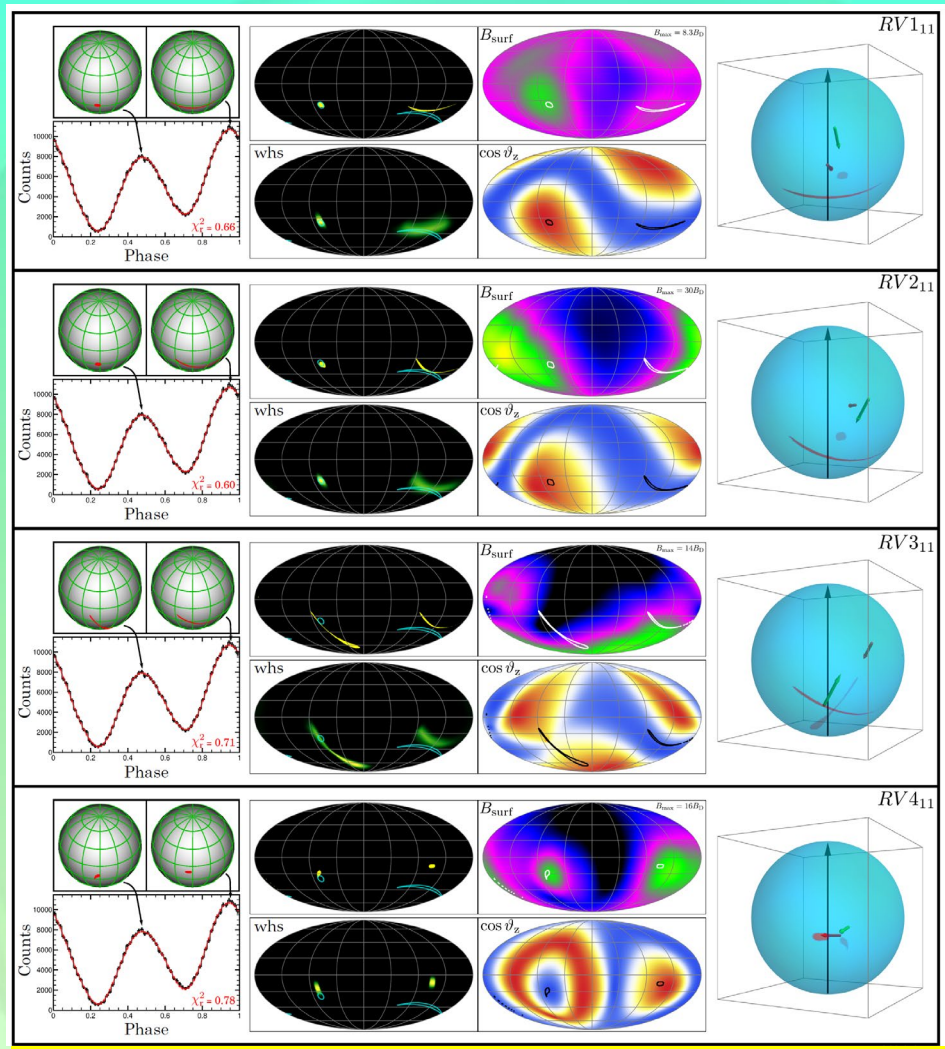

11 parameters

8 parameters

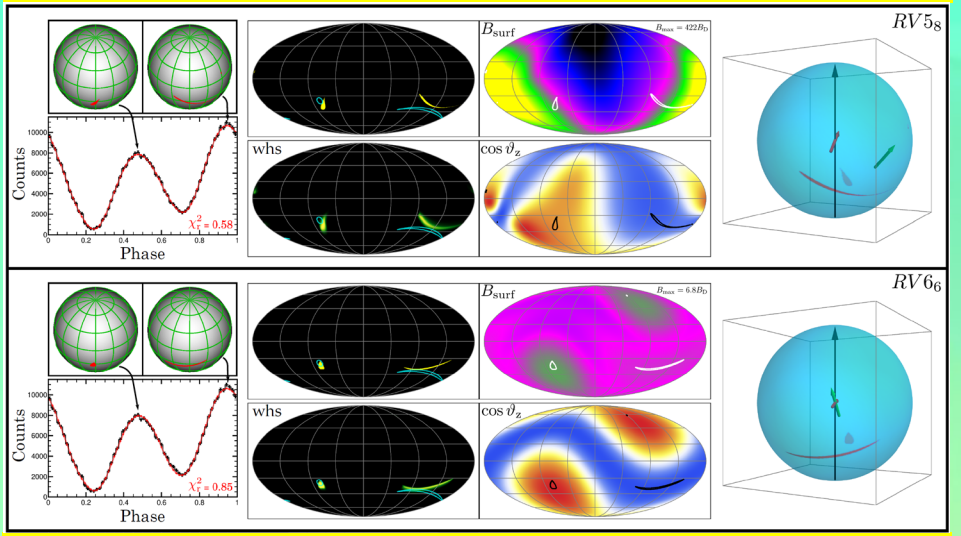

6 parameters

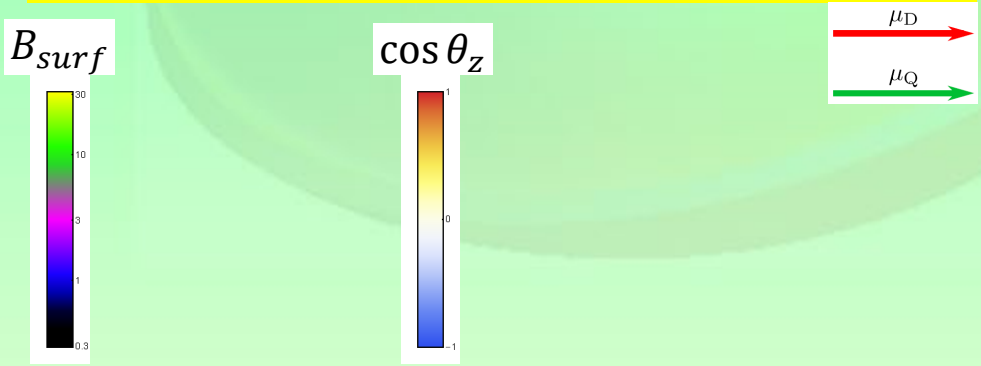

Degeneracies?

SVF, Miller et al., 2019 fixed parameters

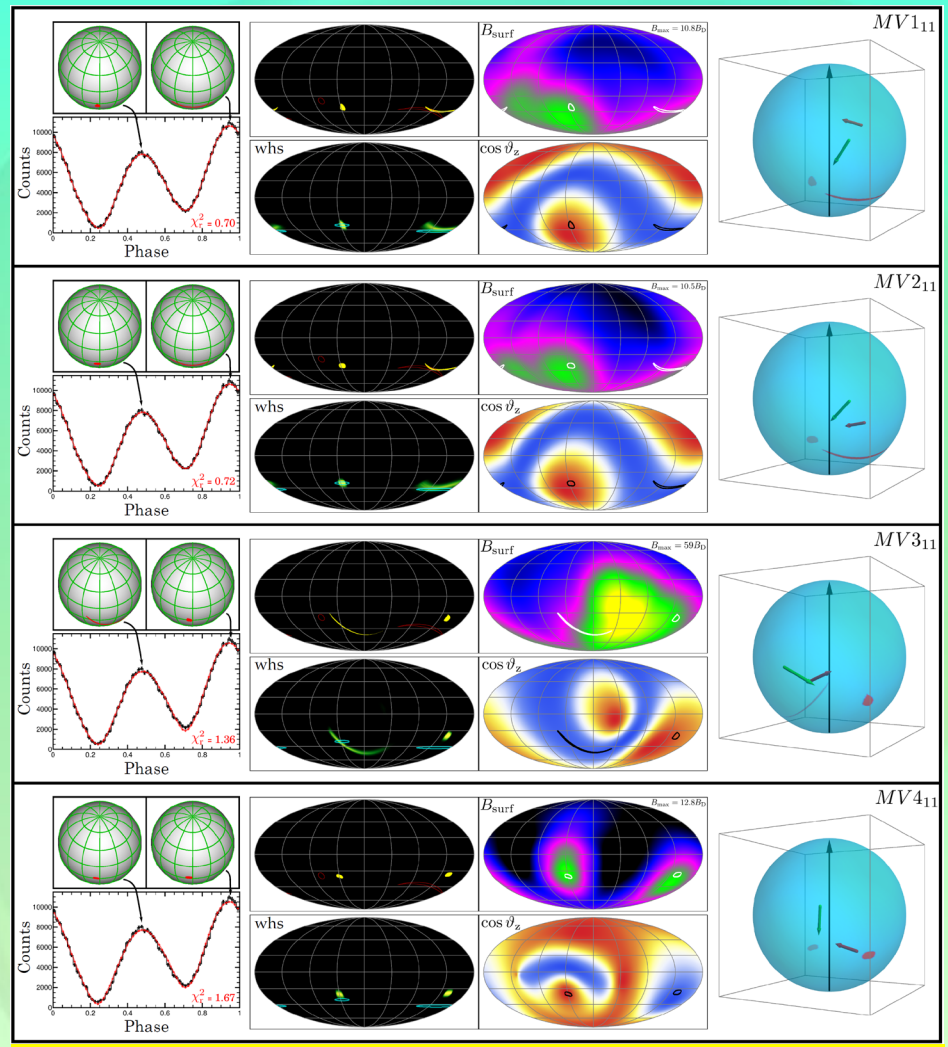

11 parameters

8 parameters

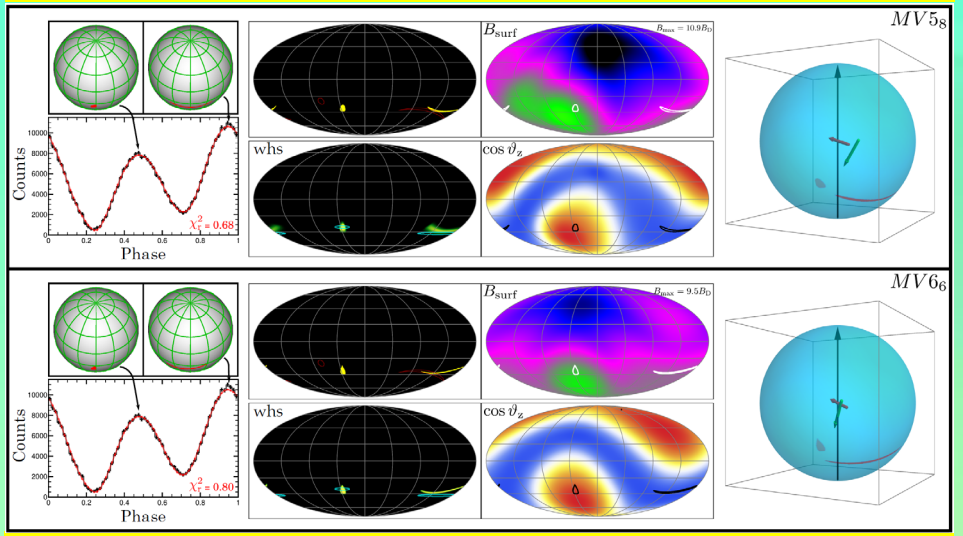

6 parameters

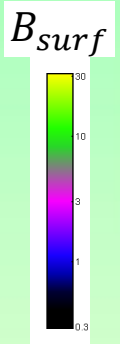

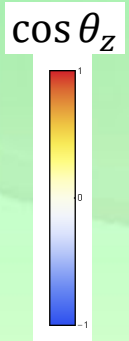

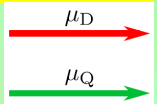

Degeneracies?

SVF model highest likelihood parameters

Quantity	$RV1_{11}$	$RV2_{11}$	$RV3_{11}$	$RV4_{11}$	$RV5_8$	$RV6_6$	$MV1_{11}$	$MV2_{11}$	$MV3_{11}$	$MV4_{11}$	$MV5_8$	$MV6_6$
$x_D(r_\star)$	0.12	0.17	0.45	−0.20	0.00	0.00	0.26	0.26	0.07	0.34	0.00	0.00
$y_D(r_\star)$	−0.17	0.39	0.29	0.46	0.00	0.00	0.12	0.22	−0.36	−0.21	0.00	0.00
$z_D(r_\star)$	−0.30	−0.04	0.11	−0.25	0.00	0.00	0.24	−0.35	−0.24	−0.40	0.00	0.00
α_D(rad)	1.75	1.60	1.98	1.53	1.00	1.38	1.38	1.72	1.29	1.45	1.40	1.35
φ_D(rad)	1.94	2.19	2.21	4.60	1.82	1.94	2.56	2.56	5.79	2.60	2.63	2.53
$x_Q(r_\star)$	0.07	0.40	0.16	0.31	0.62	0.00	0.09	0.06	−0.23	−0.36	0.09	0.00
$y_Q(r_\star)$	0.14	0.22	−0.17	−0.13	0.20	0.00	0.16	0.17	−0.37	0.36	0.19	0.00
$z_Q(r_\star)$	0.07	−0.12	−0.38	−0.15	−0.20	0.02	−0.17	−0.18	−0.25	−0.09	−0.17	−0.16
α_Q(rad)	2.18	2.29	0.60	1.68	0.92	0.75	2.34	2.18	2.04	2.60	2.38	2.42
φ_Q(rad)	1.90	2.45	6.06	4.94	5.78	4.89	2.69	2.72	0.07	2.17	2.65	2.35
B_Q/B_D	5.58	5.01	2.39	3.22	8.69	6.38	4.97	3.58	8.10	0.93	4.81	5.17
χ^2_r	0.66	0.60	0.71	0.78	0.58	0.85	0.70	0.72	1.36	1.67	0.68	0.80

Realistic FF field structures

The consensus is that the γ-rays are mainly produced outside the LC in the equatorial current sheet (ECS).

FF, Dissipative, PIC

Contopoulos & Kalapotharakos 2010
Bai & Spitkovksy 2010
Cerutti et al. 2016
Philippov & Spitkovsky 2018
Kalapotharakos et al. 2014, 2017, 2018, 2019

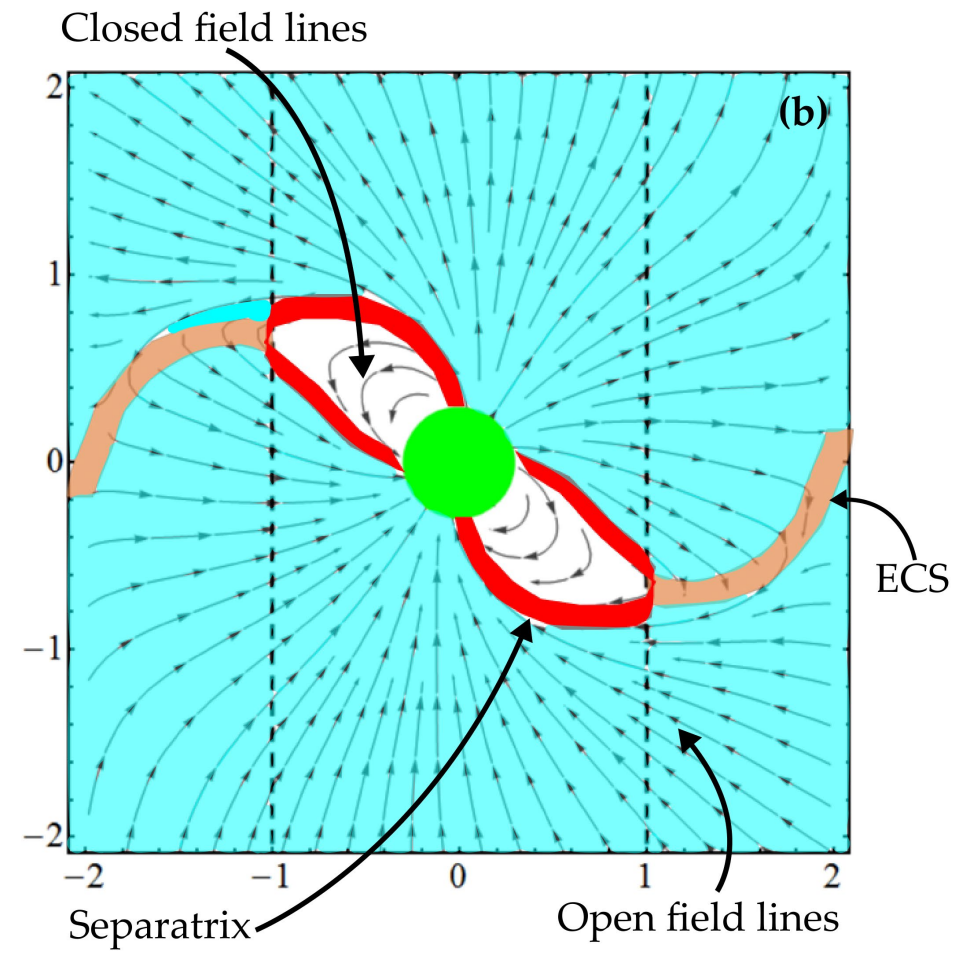

Success in reproducing Fermi gamma-ray LCs and spectra

Realistic FF/Dissipative Simulations
lifting the field degeneracies

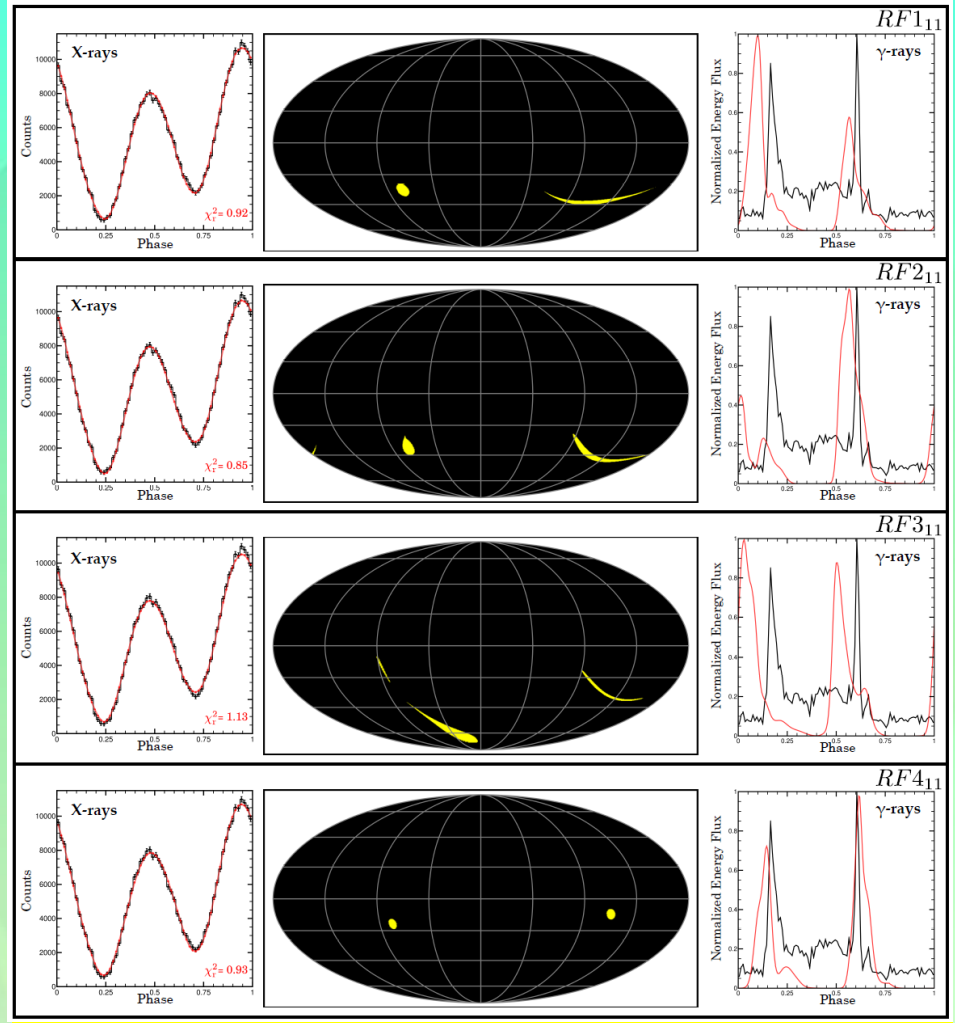

11 parameters

8 parameters

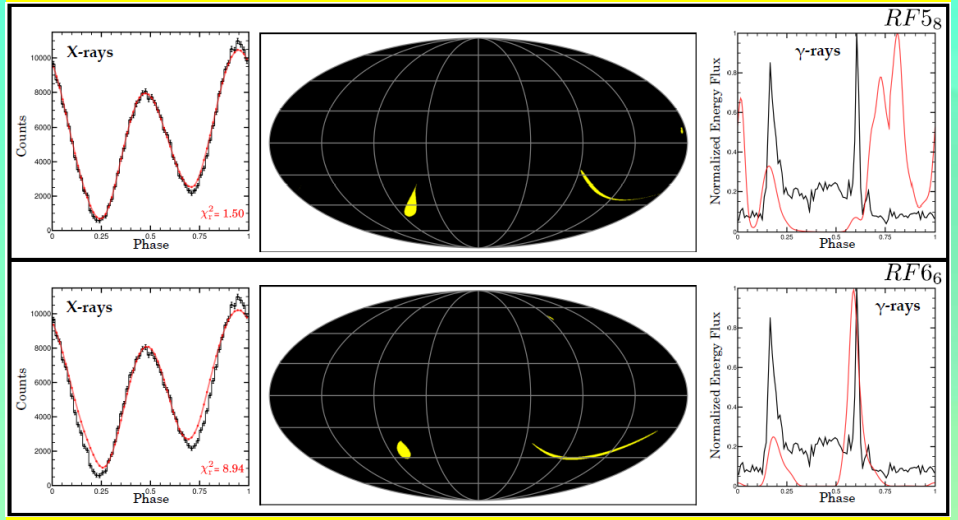

6 parameters

Fermi data

Model

FF, Riley et al., 2019 fixed parameters

3D FF field structure
γ-ray emission and X-ray thermal emission

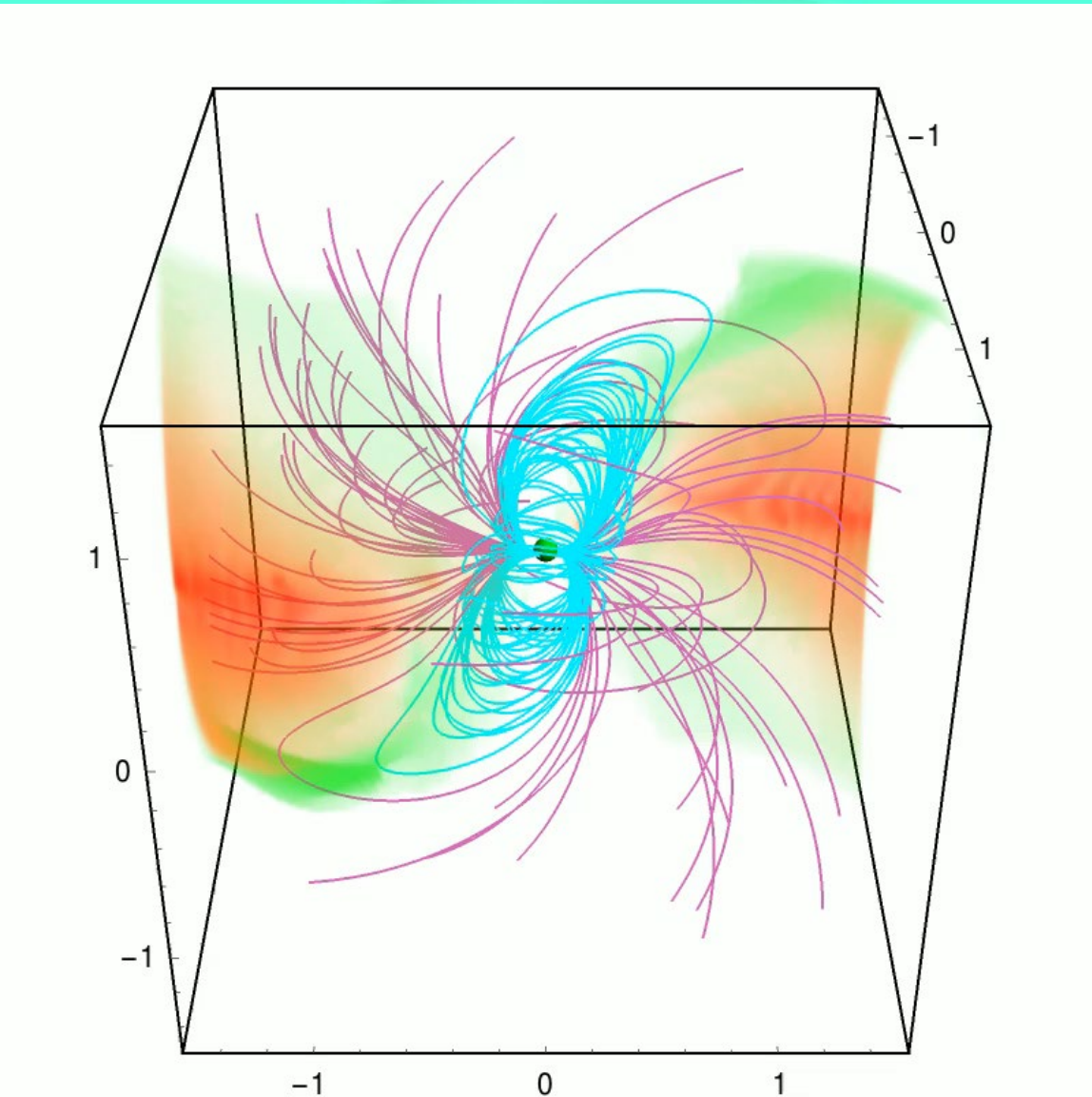

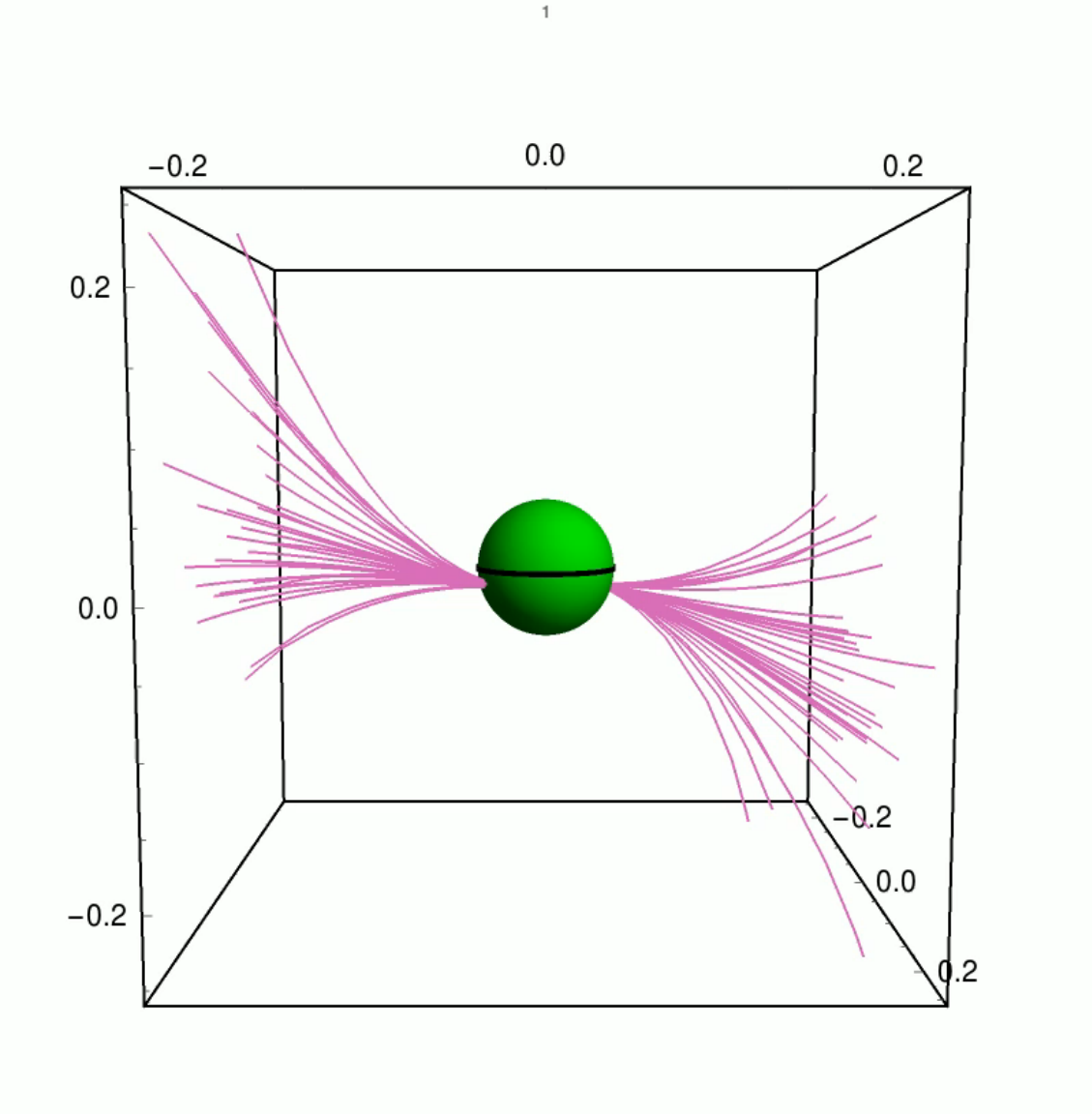

Polar cap Asymmetries
Return vs. Direct Current

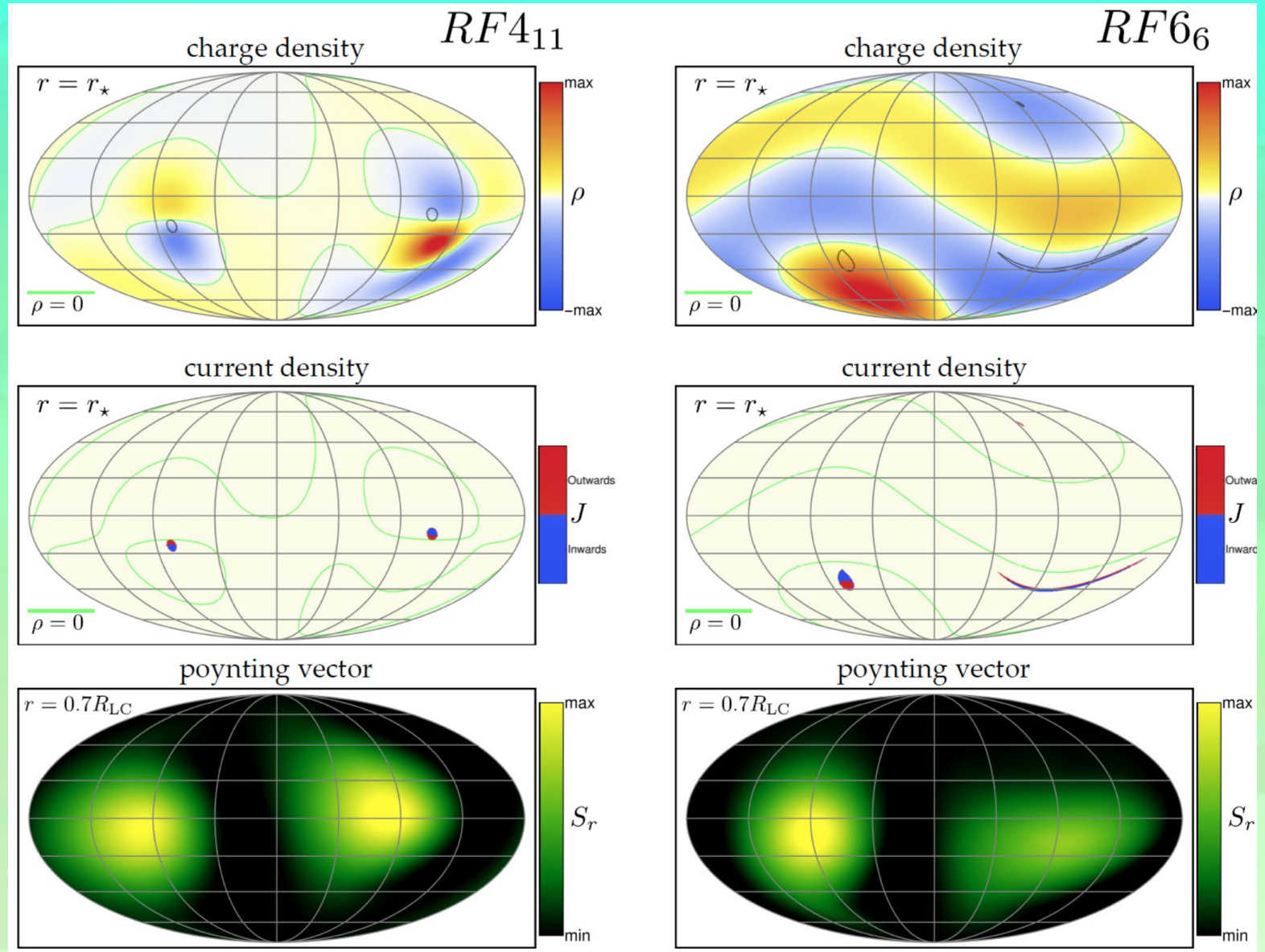

Pair production

Rocket effect

Summary

- The *NICER* thermal X-ray LC motivated us to study multipolar (D+Q) field structures in MSPs, which led to the discovery of degenerate solutions.
- Comparing the model γ-ray LCs to the *Fermi* one lifts the degeneracies.

Future

- A complete study, (i.e., MCMC exploration), which will incorporate all the related problem parameters (M_*, r_*, ζ, T), atmosphere model, energy channels, & γ-ray LCs.

Impact

Self-consistent M_*, r_*, and magnetic field determination (EoS)

Internal magnetic fields

Pair production in MSPs

Validation of the pulsar γ-ray emission model

Rocket effect

Extend the study to all the NICER MSPs